Acta Crystallographica Section D
Biological Crystallography
ISSN 1399-0047

Structure of Rot, a global regulator of virulence genes in *Staphylococcus aureus*

Yuwei Zhu,[a,b]‡ Xiaojiao Fan,[a,b]‡ Xu Zhang,[c] Xuguang Jiang,[a,b] Liwen Niu,[a,b] Maikun Teng[a,b]* and Xu Li[a,b]*

[a]Hefei National Laboratory for Physical Sciences at Microscale and School of Life Sciences, University of Science and Technology of China, Hefei, Anhui 230026, People's Republic of China, [b]Key Laboratory of Structural Biology, Chinese Academy of Sciences, Hefei, Anhui 230026, People's Republic of China, and [c]Department of Microbiology and Immunology, School of Life Sciences, University of Science and Technology of China, Hefei, Anhui 230026, People's Republic of China

‡ These authors contributed equally to this work.

Correspondence e-mail: mkteng@ustc.edu.cn, sachem@ustc.edu.cn

Received 14 May 2014
Accepted 30 June 2014

PDB reference: Rot, 4q77

Staphylococcus aureus is a highly versatile pathogen that can infect human tissue by producing a large arsenal of virulence factors that are tightly regulated by a complex regulatory network. Rot, which shares sequence similarity with SarA homologues, is a global regulator that regulates numerous virulence genes. However, the recognition model of Rot for the promoter region of target genes and the putative regulation mechanism remain elusive. In this study, the 1.77 Å resolution X-ray crystal structure of Rot is reported. The structure reveals that two Rot molecules form a compact homodimer, each of which contains a typical helix–turn–helix module and a β-hairpin motif connected by a flexible loop. Fluorescence polarization results indicate that Rot preferentially recognizes AT-rich dsDNA with ~30-base-pair nucleotides and that the conserved positively charged residues on the winged-helix motif are vital for binding to the AT-rich dsDNA. It is proposed that the DNA-recognition model of Rot may be similar to that of SarA, SarR and SarS, in which the helix–turn–helix motifs of each monomer interact with the major grooves of target dsDNA and the winged motifs contact the minor grooves. Interestingly, the structure shows that Rot adopts a novel dimerization model that differs from that of other SarA homologues. As expected, perturbation of the dimer interface abolishes the dsDNA-binding ability of Rot, suggesting that Rot functions as a dimer. In addition, the results have been further confirmed *in vivo* by measuring the transcriptional regulation of α-toxin, a major virulence factor produced by most *S. aureus* strains.

1. Introduction

Staphylococcus aureus is an important human pathogen that is capable of causing a wide range of toxin-mediated diseases such as skin infections, pneumonia, toxic shock syndrome and sepsis (Bayer *et al.*, 1996). The success of *S. aureus* as a versatile pathogen is attributable to its ability to produce wide-ranging virulence factors that facilitate tissue colonization and tissue destruction (Foster, 2005, 2009; Foster & Höök, 1998). The virulence factors of this organism can be broadly subdivided into two categories: (i) secreted proteins, such as lipases, haemolysins and proteases, that can degrade host components with antimicrobial activity and (ii) cell-wall-associated proteins, such as fibrinogen, fibronectin and collagen, that allow *S. aureus* to bind to host proteins (Lowy, 1998). The coordinated expression of these virulence factors is tightly regulated by a network of interacting regulators including two-component regulatory systems (*i.e.* Agr and SaeRS), global regulators (*i.e.* SigB, SarA and SarA

homologues) and regulatory RNA molecules (Cheung *et al.*, 1992; Dunman *et al.*, 2001; Novick & Geisinger, 2008; Liang *et al.*, 2006; Morfeldt *et al.*, 1996).

SarA (staphylococcal accessory regulator), a well studied transcriptional regulator in *S. aureus*, is vital for the regulation of various genes involved in virulence by binding to the target promoter regions (Bayer *et al.*, 1996). There are at least 11 members of the SarA family, which can be classified into three subfamilies: (i) single-domain proteins (SarA, SarR, SarT, SarV, SarX and Rot), (ii) double-domain proteins (SarS, SarU and SarY) and (iii) MarR homologues (MgrA and SarZ) (Manna *et al.*, 2004; Schmidt *et al.*, 2001; Ingavale *et al.*, 2003; Luong *et al.*, 2003; Manna & Cheung, 2003, 2006; Ballal *et al.*, 2009). The SarA family proteins are a group of DNA-binding proteins that share sequence homology with each other. To date, the crystal structure of five members of the SarA family proteins have been determined: SarA, SarR, SarS, MgrA and SarZ (Liu *et al.*, 2001, 2006; Li *et al.*, 2003; Chen *et al.*, 2006; Poor *et al.*, 2009; Sun *et al.*, 2012). These reported structures reveal that they share similar topological folds, all belonging to the winged-helix DNA-binding proteins, with helix–turn–helix and winged regions interacting with the target promoter DNA. However, owing to low sequence homology, these structures diverge significantly from each other, indicating a discrepancy between the transcription-regulation processes.

Rot (repressor of toxins), a member of the SarA family of proteins, has been characterized as a global regulator of virulence-gene expression in *S. aureus* and behaves as both a positive and a negative modulator (McNamara *et al.*, 2000; Saïd-Salim *et al.*, 2003; Tseng & Stewart, 2005; Li & Cheung, 2008). It has been reported that Rot can affect the transcription of 168 genes in *S. aureus*, some of which encode proteins that are involved in cell-surface adhesion and tissue invasion, indicating its vital role in pathogenicity (Saïd-Salim *et al.*, 2003). Rot can also work with other regulators to activate promoters, for example Rot and SaeRS, cooperatively to activate expression of the staphylococcal superantigen-like exoproteins (Benson *et al.*, 2012). However, because of a lack of structural information, how Rot binds to the promoter regions of target genes remains unknown. Here, we report the crystal structure of Rot at 1.77 Å resolution. The structure reveals that Rot exists as a homodimer in which each molecule adopts a winged-helix DNA-binding module. We confirmed the vital role of several conserved positively charged residues in the winged-helix motif in binding to dsDNA both *in vitro* and *in vivo*. In addition, our structure also shows that the pattern of dimerization of Rot is significantly different from that of the reported SarA homologues, hinting at a divergence between Rot and other SarA homologues in the transcription-regulation process.

2. Materials and methods

2.1. Construction, expression and purification

The Rot gene was PCR-amplified from *S. aureus* strain NCTC8325 using Prime STAR HS DNA Polymerase (Takara). The DNA fragment was cloned into a modified pET-28a(+) vector with a 6×His tag using the *Nde*I/*Xho*I restriction sites. All Rot mutations were generated using the MutanBEST Kit (Takara). Overexpression of all recombinant proteins was induced in *Escherichia coli* BL21 (DE3) cells (Novagen) with 0.5 m*M* isopropyl β-D-1-thiogalactopyranoside (IPTG) when the cell density reached an $OD_{600\ nm}$ of 0.6–0.8. After growth for approximately 20 h at 16°C, the cells were collected and lysed. The recombinant proteins were purified using Ni^{2+}–nitrilotriacetate affinity resin (Ni–NTA; Qiagen) in buffer (50 m*M* Tris–HCl pH 7.5, 200 m*M* NaCl, 5% glycerol) and the 6×His-Rot fusion protein was eluted with 200 m*M* imidazole. The proteins were further purified using HiTrap Q FF (5 ml) and HiLoad 16/60 Superdex 200 (GE Healthcare). The final proteins were concentrated to 43 mg ml^{-1} in buffer consisting of 20 m*M* Tris–HCl pH 7.5, 100 m*M* NaCl for crystallization trials. A selenomethionine derivative of Rot (Se-Rot) was overexpressed in the same competent cells as native Rot but using M9 medium based on a methionine-biosynthesis inhibition method. The purification of Se-Rot followed the same protocol as used for native Rot.

2.2. Crystallization, data collection and structure determination

Crystals of both native Rot (apo-Rot) and selenomethionine-derivatized Rot (Se-Rot) were grown using the hanging-drop vapour-diffusion method at 285 K and grew to maximum size in approximately 1 d in buffer consisting of 1.5 *M* ammonium chloride, 0.1 *M* sodium acetate trihydrate pH 4.6. For data collection, all crystals were soaked in a cryoprotectant solution consisting of the respective reservoir solution supplemented with 20%(*v*/*v*) glycerol and were then flash-cooled in liquid nitrogen. Data sets for all crystals were collected on beamline 17U at the Shanghai Synchrotron Radiation Facility (SSRF) at 100 K. The data were processed and scaled with *HKL*-2000 and programs from the *CCP*4 package (Winn *et al.*, 2011). The structure of Se-Rot was determined by the single-wavelength anomalous dispersion (SAD) phasing technique using *AutoSol* as implemented in *PHENIX* (Adams *et al.*, 2010). The initial model was built automatically using *AutoBuild* in *PHENIX*. Using the Se-Rot structure as the search model, the structure of apo-Rot was determined by the molecular-replacement method using *MOLREP* (Vagin & Teplyakov, 2010) as implemented in *CCP*4*i* (Winn *et al.*, 2011). All of the initial models were refined using the maximum-likelihood method implemented in *REFMAC*5 (Murshudov *et al.*, 2011) as part of the *CCP*4 program suite and rebuilt interactively using *Coot* (Emsley & Cowtan, 2004). The final models were evaluated with *MolProbity* (Chen *et al.*, 2010) and *PROCHECK* (Laskowski *et al.*, 1993). The crystallographic parameters are listed in Table 1. All of the figures showing structures were prepared with *PyMOL*.

2.3. Fluorescence polarization assays

Fluorescence polarization assays (FPAs) were performed at 298 K using a SpectraMax M5 microplate-reader system in

Table 1
Data-collection and refinement statistics for Se-Rot and apo-Rot.

Values in parentheses are for the highest resolution shell.

	Se-Rot	Apo-Rot
Data-collection statistics		
Space group	$P2_1$	$P2_1$
Unit-cell parameters (Å, °)	a = 31.7, b = 71.8, c = 65.8, $\alpha = \gamma$ = 90, β = 98.8	a = 31.7, b = 71.5, c = 65.7, $\alpha = \gamma$ = 90, β = 99.4
Wavelength (Å)	0.9791	0.9791
Resolution limits (Å)	50.00–2.00 (2.07–2.00)	50.00–1.77 (1.83–1.77)
No. of unique reflections	18795	27813
Completeness (%)	96.1 (92.9)	98.1 (99.9)
Multiplicity	7.5 (6.6)	2.8 (2.8)
R_{merge}† (%)	13.9 (30.0)	6.9 (55.1)
Mean $I/\sigma(I)$	22.2 (12.9)	18.1 (2.9)
Refinement statistics		
Resolution limits (Å)		32.42–1.77
R_{work}‡/R_{free}§ (%)		16.32/21.72
R.m.s.d., bonds (Å)		0.007
R.m.s.d., angles (°)		1.089
B factor (Å^2)		
Protein		31.74
Water		39.45
No. of non-H protein atoms		2146
No. of water O atoms		140
Ramachandran plot (%)		
Most favoured regions		95.7
Additional allowed regions		3.8
Generously allowed regions		0.4
PDB entry		4q77

† $R_{merge} = \sum_{hkl}\sum_i |I_i(hkl) - \langle I(hkl)\rangle|/\sum_{hkl}\sum_i I_i(hkl)$, where $I_i(hkl)$ is the ith observation of reflection hkl and $\langle I(hkl)\rangle$ is the weighted average intensity for all i observations of reflection hkl. ‡ $R_{work} = \sum_{hkl} ||F_{obs}| - |F_{calc}||/\sum_{hkl} |F_{obs}|$, where F_{obs} and F_{calc} are the observed and calculated structure factors for reflection hkl, respectively. § R_{free} was calculated in the same way as R_{work} but using a randomly selected 5% of the reflections which were omitted from refinement.

buffer consisting of 20 m*M* Tris–HCl pH 7.5, 100 m*M* NaCl. The wavelengths of fluorescence excitation and emission were 490 and 524 nm, respectively. Each well of a 384-well plate contained 100 n*M* fluorescent-labelled (5′-FAM) DNA probe and different amounts of Rot or Rot mutant with a final volume of 80 µl. For each assay, DNA-free controls were included. The fluorescence polarization P (in mP units) was calculated as

$$P = (I_{\parallel} - I_{\perp})/(I_{\parallel} + I_{\perp}). \quad (1)$$

The fluorescence polarization change ΔP (in mP units) was fitted to

$$\Delta P = \Delta P_{max} \times [\mathrm{Rot}]/(K_d + [\mathrm{Rot}]). \quad (2)$$

The binding curves were fitted according to a one-site binding model using the *Origin* software. The dsDNA probe used in the assays was formed by annealing ssDNA with complementary ssDNA. The sequences of the 5′-FAM-labelled DNA probe are described in Supplementary Table S1.[1]

[1] Supporting information has been deposited in the IUCr electronic archive (Reference: QH5011).

2.4. Size-exclusion chromatography assay

The apparent molecular masses of Rot and the Rot-M9 mutant (see §3.5) were estimated with a Superdex 200 column (10/300 GL; GE Healthcare). Briefly, protein samples or molecular-mass standards were applied onto the Superdex 200 column at a flow rate of 0.6 ml min^{-1} and eluted with 50 m*M* Tris–HCl pH 7.5, 100 m*M* NaCl. The standard proteins (GE Healthcare) used in this assay were β-amylase (200.0 kDa), alcohol dehydrogenase (150.0 kDa), albumin (66.0 kDa), carbonic anhydrase (29.0 kDa) and cytochrome *c* (12.4 kDa). The void volume was determined with blue dextran (GE Healthcare).

2.5. Complementation of the *rot* knockout strain

The *rot* knockout strain SX21 was kindly provided as a gift by Dr Baolin Sun. All the complementary plasmids of different *rot* mutants were generated using the MutanBEST kit (Takara) using the plasmid pLI50-rot as a template. These recombinant plasmids were transformed into *S. aureus* RN4220 and then electroporated into the *rot* knockout strain SX21 (Xue *et al.*, 2012).

2.6. Western blot

A Western blot of α-toxin was performed as described previously (Xue *et al.*, 2014). Briefly, the same amount of stationary-phase supernatant of the wild type, the *rot* knockout stain and the complementary strains of different *rot* mutants were collected and concentrated by 10 kDa ultrafiltration (Millipore). These samples were then separated by 12% SDS–PAGE and electrotransferred onto a polyvinylidene difluoride membrane (GE). Finally, α-toxin was detected by a rabbit anti-α-toxin antibody (Sigma) followed by horseradish peroxidase-conjugated sheep anti-rabbit antibodies (Pierce).

3. Results

3.1. The DNA-binding properties of Rot

Although Rot, a SarA homologue, was previously identified as a global regulator of virulence genes in *S. aureus*, the DNA-recognition model of Rot for the target promoter region remains unknown. To investigate the DNA-binding properties of Rot, we performed a fluorescence polarization assay (FPA) to test the binding affinities of Rot for different lengths of dsDNA. As shown in Fig. 1(*a*), Rot displayed no binding affinity for 7 bp AT-rich dsDNA, but could bind to AT-rich dsDNAs longer than 24 bp. The K_d value for the binding of Rot to 24 bp AT-rich dsDNA was 32.47 µ*M* and the K_d value increased to 19.87 and 7.30 µ*M* when binding to 28 bp AT-rich dsDNA and 38 bp AT-rich dsDNA, respectively. Next, we examined whether Rot had a sequence preference; as shown in Fig. 1(*a*), no obvious binding affinity of Rot to 24 bp GC-rich dsDNA was observed. Our results suggested that Rot preferentially recognizes AT-rich dsDNAs with ∼30 bp nucleotides and were consistent with the previously reported

crystal structures of SarA homologues, which revealed that the longest distance for two winged-helix motifs could accommodate a B-form dsDNA with ∼27 bp nucleotides (Liu *et al.*, 2001, 2006; Li *et al.*, 2003).

3.2. Overall structure of Rot

To improve the understanding of the DNA-recognition model of Rot, we determined the crystal structure of Rot at 1.77 Å resolution. The structure was solved by SAD phasing and molecular replacement. The crystallographic statistics are summarized in Table 1. The monomeric Rot adopts an L-shaped structure (Fig. 1*b*). There are two Rot molecules in one asymmetric unit, which form a homodimer through extensive hydrophobic interactions (Fig. 1*b*). Rot displays a similar topology to the structures of SarA and SarR, consisting of five α-helices and three β-strands. The arrangement of the secondary-structure elements in each monomer is $\alpha1$–$\alpha2$–$\beta1$–$\alpha3$–$\alpha4$–$\beta2$–$\beta3$–$\alpha5$ (Figs. 1*b* and 1*c*). Helices $\alpha1$ and $\alpha2$ are oriented perpendicular to each other (Fig. 1*b*). Helices $\alpha1$ and $\alpha5$ from each monomer bring the two Rot molecules together (Fig. 1*b*). Interestingly, helix $\alpha5$ of Rot is longer than that of

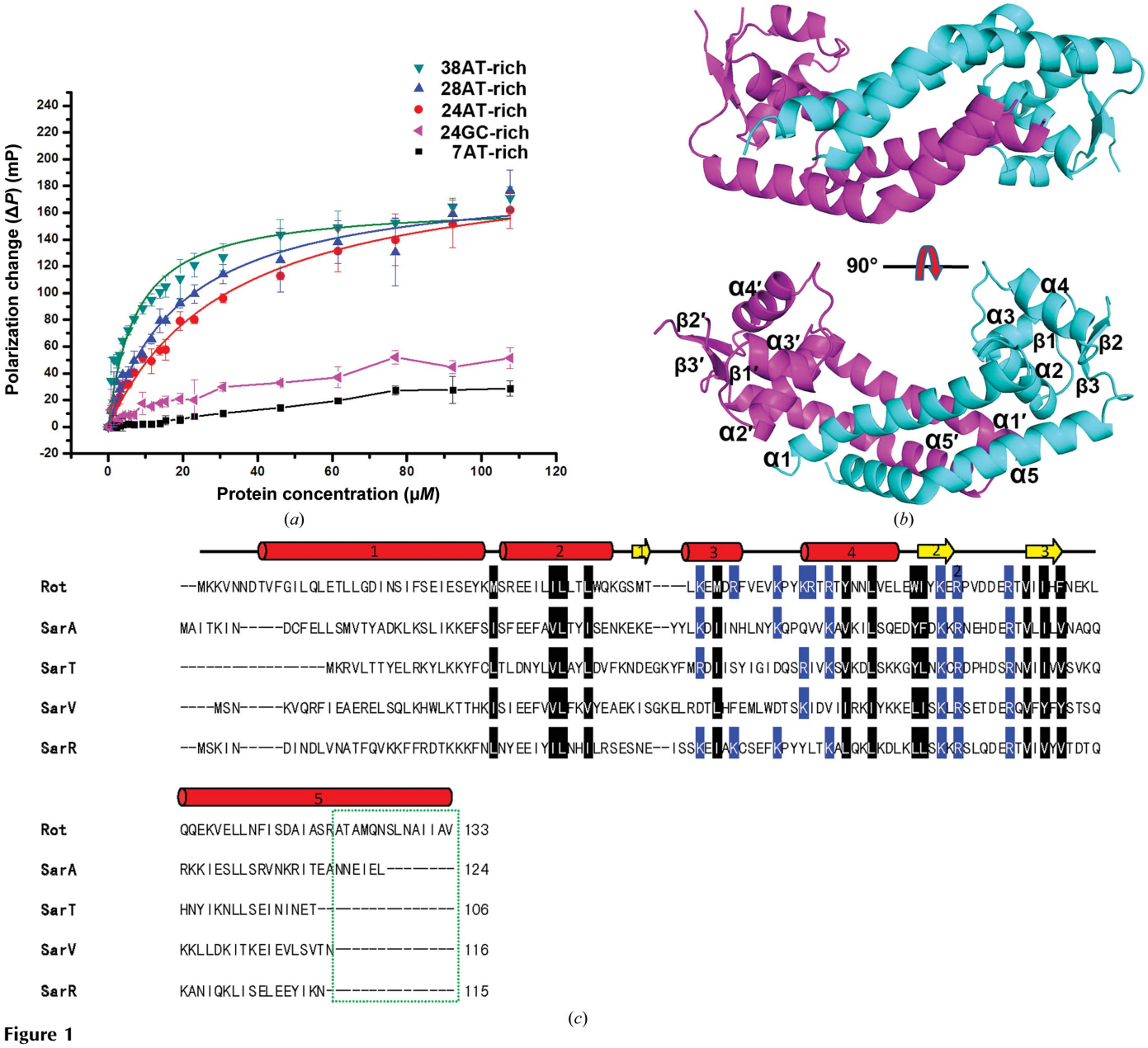

Figure 1
Overall structure of Rot and its DNA-binding properties. (*a*) Fluorescence polarization assay of the interaction of Rot with dsDNA oligonucleotides of different lengths. (*b*) Two views of the Rot dimer. Monomer *A* is shown as a cartoon coloured magenta and monomer *B* is coloured cyan. (*c*) Sequence alignment of Rot, SarA, SarT, SarV and SarR. The secondary-structural elements of Rot are shown at the top of the sequence. α-Helices are coloured red and β-strands are coloured yellow. The conserved hydrophobic residues involved in building up the large hydrophobic environment to sustain the winged-helix motif are highlighted in black. The residues involved in binding to DNA are highlighted in blue. The sequence extension (residues 120–133) at the tail of Rot is marked by a green box.

other single-domain SarA homologues, which is caused by a sequence extension (residues 120–133) at the tails of the Rot molecules, which form a coiled coil with each other (Figs. 1*b* and 1*c*). In addition, helices α3 and α4 form the typical helix–turn–helix motif, a widely existing DNA-binding module (Fig. 1*b*). β2 and β3 form a β-hairpin constituting the winged motif (Fig. 1*b*). The DNA-binding winged-helix motifs from each monomer are separated by approximately 43 Å, which is similar to that in SarA, SarR and SarS but is significantly different from that in the MarR homologues MgrA and SarZ (Liu *et al.*, 2001, 2006; Li *et al.*, 2003; Chen *et al.*, 2006; Poor *et al.*, 2009). Owing to the distinct pattern of dimerization, the winged-helix motifs in MgrA and SarZ are separated by only 14 Å (Chen *et al.*, 2006; Poor *et al.*, 2009). Large differences can also be found in the loop region connecting the β-hairpin, which is missing because of flexibility (residues 87–91) but is well defined in the structures of SarA, SarR and SarS. It is worth noting that surrounding the winged-helix motifs, a large number of hydrophobic residues build up a large hydrophobic environment to form a compact and rigid structure, indicating the vital role of these elements in target DNA recognition (Figs. 1*b* and 1*c*).

3.3. The interaction between Rot and DNA

Consistent with the SarA family proteins, Rot contains a high percentage of positively charged residues, which are mainly accumulated on the winged-helix motifs (Figs. 1*a* and 1*b*). Sequence alignment revealed that these positively charged residues were conserved among SarA homologues (Fig. 1*c*). Next, we performed a fluorescence polarization experiment (FPA) to investigate which residues in the winged-helix motifs were important for recognition of the target DNA. We produced eight Rot mutants, Rot-M1 (Lys55 mutated to Ala), Rot-M2 (Arg59 mutated to Ala), Rot-M3 (Lys64 mutated to Ala), Rot-M4 (Lys67, Arg68 and Arg70 mutated to Ala), Rot-M5 (Lys83 mutated to Ala), Rot-M6 (Arg85 mutated to Ala), Rot-M7 (Arg91 mutated to Ala) and Rot-M8 (Tyr66 mutated to Ala) and tested their abilities to bind to 38 bp AT-rich dsDNA (Fig. 2*b*). As shown in Fig. 2(*c*),

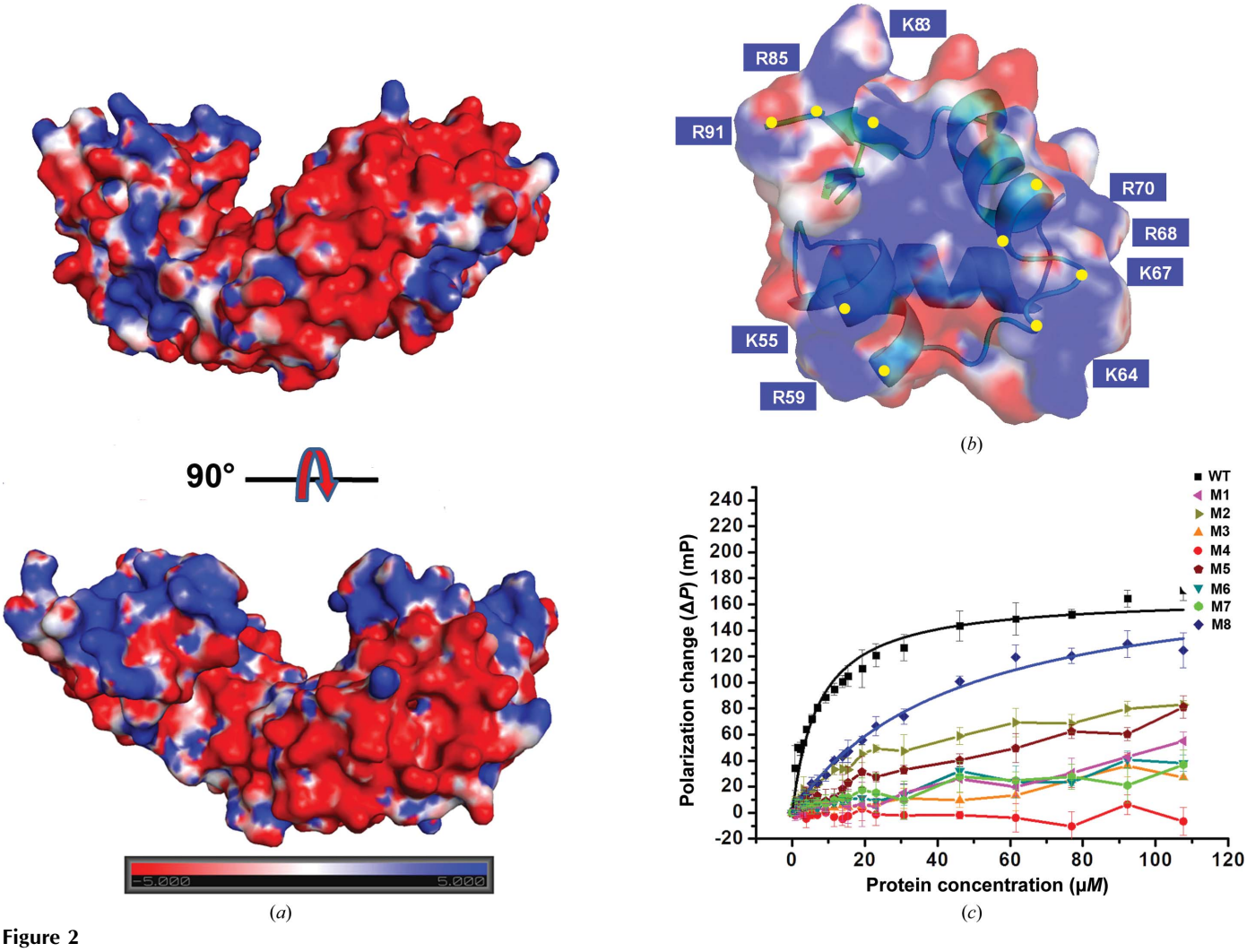

Figure 2
The interaction between Rot and dsDNA. (*a*) Two electrostatic potential surface views of the Rot dimer. (*b*) The conserved positively charged residues in the helix–turn–helix and β-hairpin regions are labelled and highlighted in yellow. (*c*) Fluorescence polarization assay of Rot and mutants with a 5′-FAM-labelled 38 bp AT-rich dsDNA.

the dsDNA-binding ability of the Rot mutants (Rot-M1–Rot-M7) decreased significantly compared with that of wild-type Rot (WT-Rot), indicating that these conserved positively charged residues in the winged-helix motifs were vital for recognition of the target dsDNA and were most likely involved in interaction with the DNA phosphate backbone. Interestingly, Tyr66 in the loop region connecting β2 and β3 also played an important role in DNA binding, and the DNA-binding affinity of this mutant decreased sevenfold compared with that of WT-Rot. It is worth noting that this residue (Tyr66) was not conserved among the SarA homologues (Fig. 1*c*). Taken together, we propose that the residues in the winged-helix motifs from each monomer are necessary for Rot to bind to target dsDNA, which is similar to the case in other SarA homologues, but a subtle difference exists in the residues involved in binding to the dsDNA.

3.4. Unique pattern of dimerization

As discussed above, Rot exists as a homodimer in the asymmetric unit, similar to SarA, SarR, MgrA and SarZ (Liu *et al.*, 2001, 2006; Chen *et al.*, 2006; Poor *et al.*, 2009). However, the pattern of dimerization of Rot was significantly different from that of the reported SarA homologues. Based on the structures reported previously, we found that the pattern of dimerization of SarA family proteins could be divided into two classes. As shown in Fig. 3, the single-domain proteins SarA and SarR and the double-domain protein SarS represent a universal pattern of dimerization of SarA homologues, in which α1 of one monomer inserts into the hydrophobic pocket formed by α1, α2 and α5 of the other monomer. This differed from another two SarA homologues, MgrA and SarZ, which contained structural features similar to those of MarR instead of the SarA homologues (Chen *et al.*, 2006; Poor *et al.*, 2009). In the structures of MgrA and SarZ, the dimerization interfaces were mediated by two hydrophobic pockets through domain swapping, in which α1 of one monomer inserts into the hydrophobic pocket formed by α1, α5 and α6 of the other monomer and forms a coiled coil with α6 of the other monomer (Chen *et al.*, 2006; Poor *et al.*, 2009; Fig. 3). Interestingly, the crystal structure of Rot, a single-domain SarA homologue, revealed a novel pattern of dimerization. The structure suggested that both α1 and α5 from one monomer insert into the hydrophobic pocket formed by α1, α2 and α5 from the other monomer (Fig. 3). The interaction was further strengthened by sequence extensions (residues 120–133) at the tail of the Rot molecules, which formed a coiled coil with each other through hydrophobic interactions (Fig. 4*a*). The interactions between the two monomers were quite extensive, burying $\sim$2870 Å^2 of solvent-accessible surface area. Residues Val9, Ile12, Leu13, Leu15, Leu18, Ile22, Ile25 and Phe26 from α1, residues Leu44 and Trp47 from α2 and residues Ile112, Ile116, Ala120, Met123, Leu127 and Ile131 from α5 of each monomer were involved in the hydrophobic dimer interface (Fig. 4*a*). In addition, Gln124 from each monomer contributed two hydrogen bonds (Fig. 4*a*).

3.5. Rot functions as a dimer

Previous work has demonstrated that SarA homologues such as SarA, SarR, MgrA and SarZ all crystallize as a homodimer, indicating that a dimer may be the smallest

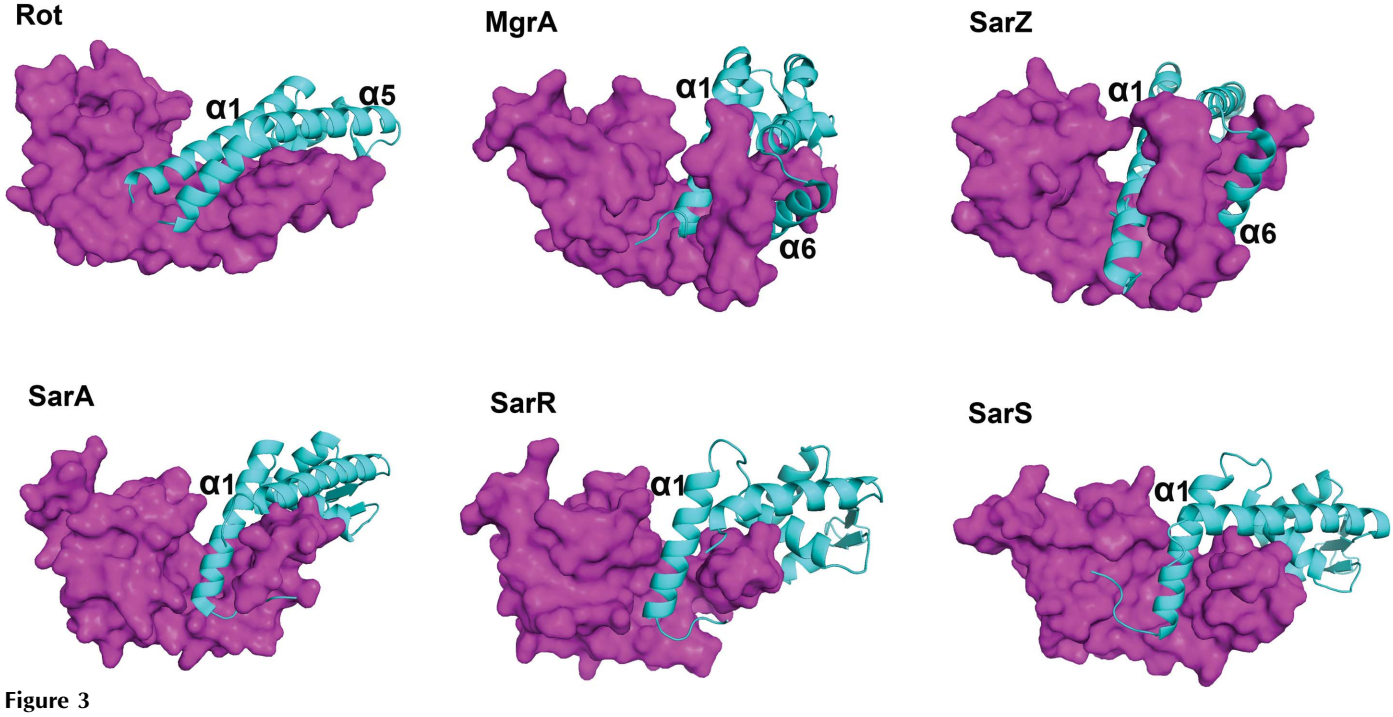

Figure 3
Distinct patterns of dimerization of SarA homologues. Dimer views of Rot and other SarA homologues (SarA, SarR, SarS, MgrA and SarZ). Monomer *A* is coloured magenta and shown as a surface representation and monomer *B* is shown as a cartoon and coloured cyan.

functional unit of this family of proteins (Liu *et al.*, 2001, 2006; Chen *et al.*, 2006; Poor *et al.*, 2009). However, there was still not sufficient evidence to support this notion. To test it, we produced a mutant Rot-M9 (Met123, Leu127 and Ile131 mutated to Ala) to disrupt the dimer interface and compared the DNA-binding ability of Rot-M9 with that of WT-Rot. First, we performed a size-exclusion chromatographic assay, as shown in Fig. 4(*b*), in which WT-Rot eluted with a molecular weight of approximately 44.6 kDa, which was larger than the theoretical value of 31.2 kDa for the Rot dimer. Considering the oblong rather than globular shape of Rot, we thought that this was credible. As expected, Rot-M9 eluted with a molecular weight of 25.6 kDa, which was approximately half of 44.6 kDa, indicating that Rot-M9 existed as a monomer. Next, we performed a fluorescence polarization assay to compare the DNA-binding affinity of Rot-M9 with that of WT-Rot. As shown in Fig. 4(*c*), the DNA-binding ability of Rot-M9 decreased significantly compared with that of WT-Rot, indicating that a dimer was the smallest functional unit of Rot that can contact DNA.

3.6. Repression of *α*-toxin by Rot

α-Toxin is a pore-forming toxin that has cytolytic, haemolytic and dermonecrotic activities and has been reported to be down-regulated by Rot (Xue *et al.*, 2014; Li & Cheung, 2008). To confirm that the residues involved in interaction with DNA also functioned *in vivo*, we assayed the level of transcriptional repression of *α*-toxin by WT-Rot and Rot mutants (Rot-M1–Rot-M8). As shown in Fig. 5, the expression of *α*-toxin was extremely suppressed by WT-Rot, which could be detected in the *rot* knockout strain SX21. As expected, Rot mutants failed to repress the expression of *α*-toxin except for Rot-M2 (Fig. 5). We speculated that Arg59 may not play an important role in interacting with DNA *in vivo*, which was consistent with the observation that the DNA-binding ability of Rot-M2

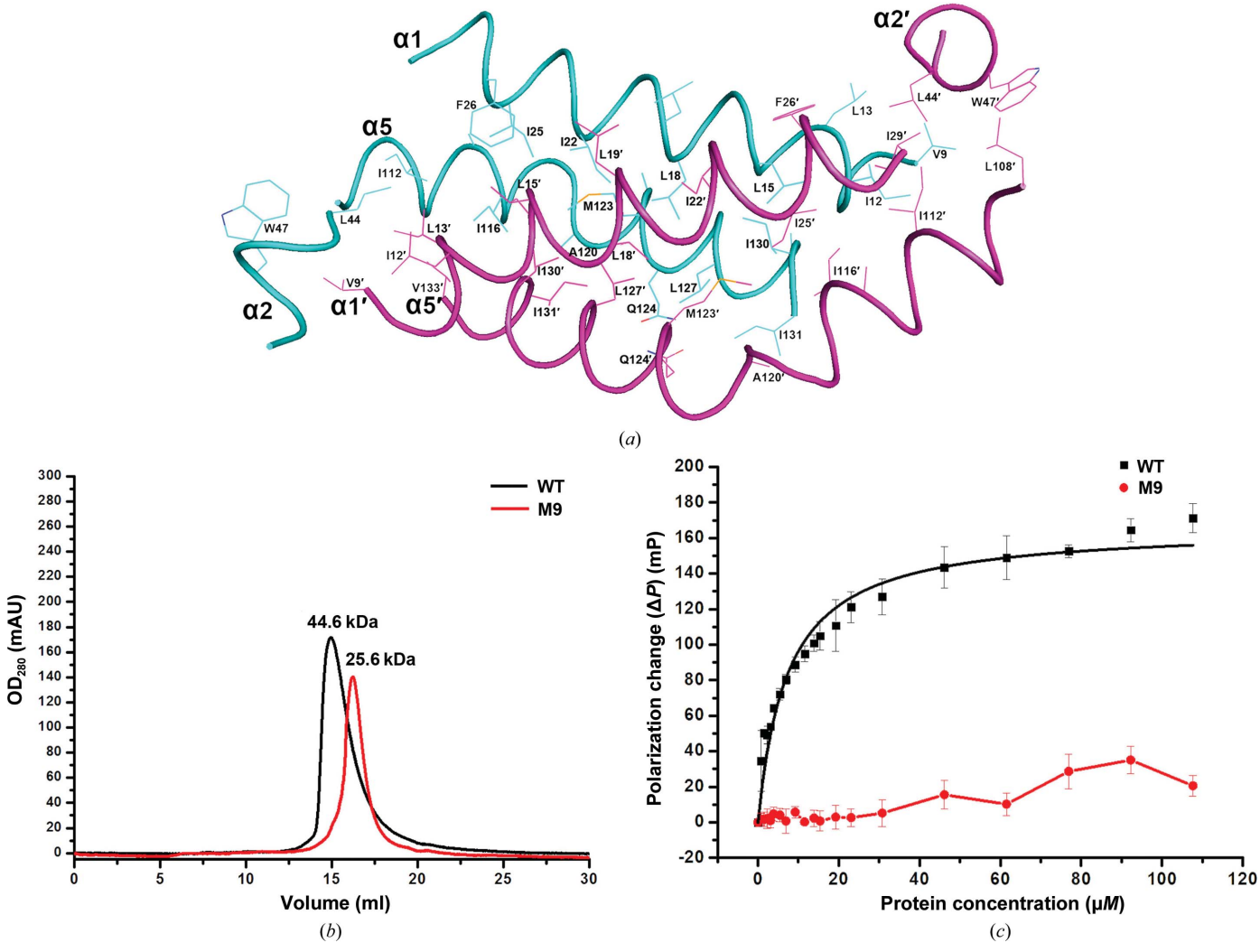

Figure 4
Rot functions as a dimer. (*a*) The dimerization interface of Rot; the residues involved in the dimerization interaction are labelled and coloured as in Fig. 1(*b*). (*b*) Gel-filtration analysis of WT-Rot and a Rot mutant; WT-Rot and Rot-M9 elute with molecular weights of approximately 44.6 and 25.6 kDa, respectively. (*c*) Fluorescence polarization assay of WT-Rot and Rot-M9 with a 5′-FAM-labelled 38 bp AT-rich dsDNA.

displayed a slight decrease compared with that of other Rot mutants (Rot-M1–Rot-M7). Next, we further confirmed that destruction of the dimerization of Rot (Rot-M9) affected the transcriptional repression of α-toxin *in vivo* (Fig. 5). In brief, these data strongly supported the *in vitro* assay results.

4. Discussion

4.1. Putative Rot–dsDNA recognition model

To reveal the structural similarities and differences between Rot and other SarA homologues, we compared the structure of Rot with those of SarA, SarR and MgrA. The overall main-chain r.m.s.d. between Rot and SarA was 3.886 Å for 101 comparable C^{α} atoms (Supplementary Fig. S1*b*). Because of structural divergence, we were unable to compare the winged-helix motif of Rot with that of SarA. The overall main-chain r.m.s.d. between Rot and SarR was 2.165 Å for 73 comparable C^{α} atoms and the r.m.s.d. of the winged-helix motif was 1.917 Å for 35 comparable C^{α} atoms (Supplementary Fig. S1*c*). The overall main-chain r.ms.d. between Rot and MgrA was 4.542 Å for 102 comparable C^{α} atoms and the r.m.s.d. of the winged-helix motif was 6.555 Å for 29 comparable C^{α} atoms (Supplementary Fig. S1*d*). As described previously, Rot preferentially recognized dsDNA with ∼30 bp nucleotides, and the winged-helix motif was responsible for the recognition of the target DNA by Rot. Our data supported a model in which helix α4 from each monomer of Rot inserts into the major grooves of the target DNA and the loops between β2 and β3 directly contacted the minor grooves, similar to the DNA-recognition model observed in the structure of MarR family proteins such as MepR, Sco3205, OhrR and ST1710 (Birukou *et al.*, 2014; Stevenson *et al.*, 2013; Hong *et al.*, 2005; Kumarevel *et al.*, 2009). In addition, a slight rearrangement of the winged-helix motif was also required to better accommodate the target DNA. However, the structure of the complex of Rot with DNA was still needed to confirm our hypothesis.

4.2. Rot represents a novel type of dimerization

As discussed above, the single-domain SarA homologues have been classified into two subfamilies. In the first subfamily, five helices and three short β-strands built up a global domain, such as in SarA and SarR, in which α1 of one monomer inserts into the hydrophobic pocket formed by α1, α2 and α5 of the other monomer (Liu *et al.*, 2006; Liu *et al.*, 2001; Fig. 3). In the second subfamily, there was an additional helix at the C-terminus, for example in the MarR homologues MgrA and SarZ (Chen *et al.*, 2006; Poor *et al.*, 2009). In addition to α1, this additional helix (α6) further strengthens the monomer–monomer interaction by inserting into the hydrophobic pocket formed by α1 and α6 of the other monomer (Fig. 3). Surprisingly, Rot adopted a similar topology to the single-domain SarA homologues SarA and SarR but displayed a significantly different mode of dimerization. The structure of Rot revealed that both α1 and α5 from one monomer insert into the hydrophobic pocket formed by α1, α2 and α5 from the other monomer. Combining the previously reported structures of SarA homologues, we proposed that the distinct pattern of dimerization of Rot was mainly caused by the orientation of helices α1–α5. In each monomer structure of Rot, helix α1 was oriented approximately perpendicular to helix α5, differing significantly from the other SarA homologues, in which helices α1 and α5 were oriented approximately 120° to each other. In addition, there was a sequence extension (residues 120–133) at the tail of Rot compared with the other single-domain SarA homologues; these formed a coiled coil with each other through hydrophobic interaction. Consequently, we strongly suggest that Rot should be classified into a novel subfamily.

4.3. Distinct types of dimerization may hint at distinct regulation mechanisms

Previous studies have reported that Rot is an important transcriptional regulator in *S. aureus*; however, how this transcription factor carries out this function remained unknown. Several years ago, Ptashne and Gann proposed that transcription activators work by bringing the transcriptional machinery to the DNA for gene activation, and many transcription activators have been reported to activate transcription *via* protein–protein contact between the transcription apparatus and transcription factors (Ptashne & Gann, 1997). For example, cyclic AMP receptor regulates downstream protein expression through interacting with the C-terminal domains of the α subunit of RNA polymerase in *Escherichia coli* (Ishihama, 1993). Similarly, deletion of the α subunit of RNA polymerase suppressed the transcriptional activation of FlhD/FlhC (Liu *et al.*, 1995). According to this theory, transcription-activating proteins should have two structural motifs: a DNA-binding motif and an activation motif. Previous studies discovered that in the structures of SarA, SarR and SarS there was an acidic patch on the convex side in each monomer which possibly acted as an activation motif to recruit RNA polymerase to the promoter region *via* direct electrostatic interaction with a positively charged surface of the RNA polymerase subunit (Liu *et al.*, 2001, 2006; Li *et al.*, 2003). To probe the putative function of the novel mode of dimerization of Rot, we compared the convex side of Rot with that of SarA homologues. Surprisingly, we found that

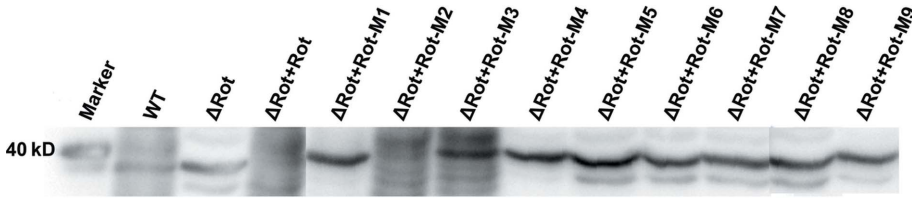

Figure 5
Western blot analysis of α-toxin in *S. aureus* RN6911 (WT), the *rot* knockout strain and rescue strains of Rot and Rot mutants.

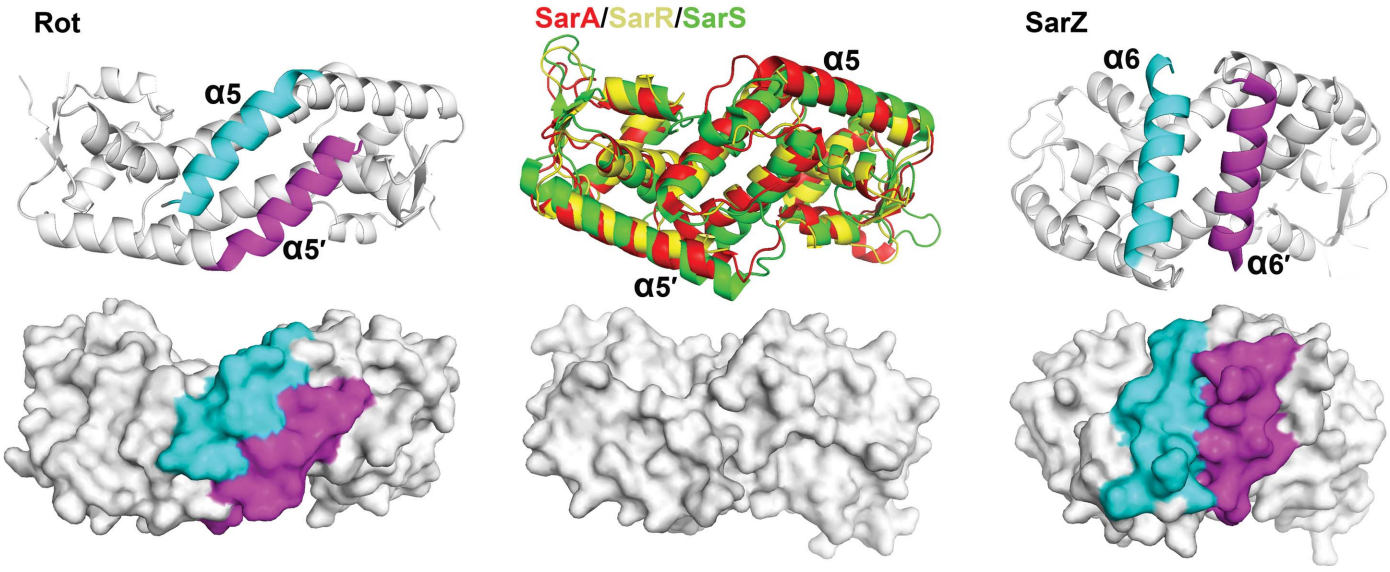

Figure 6
Surface view of the putative transcription-activation motif of SarA homologues. α6 of SarZ and α5 of Rot are coloured magenta and cyan in each monomer. The cartoon views of SarA, SarR and SarS are coloured red, yellow and green, respectively.

the two convex sides were separated in Rot by the tail of helix α5 (residues 120–133) of each monomer but formed a continuous interface in the structures of SarA, SarR and SarS (Fig. 6). Similarly, the two convex sides were also separated in the structures of MgrA and SarZ by helix α6 of each monomer (Fig. 6). However, helix α6 was oriented approximately perpendicular to helix α5 in each monomer of MgrA and SarZ, but the tail of helix α5 was oriented approximately 150° to the head in each monomer of Rot (Fig. 6). In addition, the conformation of the Rot dimer was more extended than those of MgrA and SarZ (Fig. 6). These studies revealed that the distinct types of dimerization of SarA homologues causes a distinct interface that may function in the recruitment of RNA polymerase, indicating that the putative regulation process may differ between Rot and other SarA homologues. However, the details of protein–protein communication between SarA homologues and the transcription apparatus are still unknown, and further studies are still needed to verify this hypothesis.

We thank the staff of BL17U at SSRF for assistance with synchrotron diffraction data collection. Financial support for this project was provided by the Chinese National Natural Science Foundation (Grant No. 31130018), the Chinese Ministry of Science and Technology (Grant No. 2012CB917200), the Chinese National Natural Science Foundation (Grant Nos. 31370732 and 31270014) and the Science and Technological Fund of Anhui Province for Outstanding Youth (Grant No. 1308085JGD08).

References

Adams, P. D. *et al.* (2010). *Acta Cryst.* D**66**, 213–221.
Ballal, A., Ray, B. & Manna, A. C. (2009). *J. Bacteriol.* **191**, 1656–1665.
Bayer, M. G., Heinrichs, J. H. & Cheung, A. L. (1996). *J. Bacteriol.* **178**, 4563–4570.
Benson, M. A., Lilo, S., Nygaard, T., Voyich, J. M. & Torres, V. J. (2012). *J. Bacteriol.* **194**, 4355–4365.
Birukou, I., Seo, S. M., Schindler, B. D., Kaatz, G. W. & Brennan, R. G. (2014). *Nucleic Acids Res.* **42**, 2774–2788.
Chen, P. R., Bae, T., Williams, W. A., Duguid, E. M., Rice, P. A., Schneewind, O. & He, C. (2006). *Nature Chem. Biol.* **2**, 591–595.
Cheung, A. L., Koomey, J. M., Butler, C. A., Projan, S. J. & Fischetti, V. A. (1992). *Proc. Natl Acad. Sci. USA*, **89**, 6462–6466.
Chen, V. B., Arendall, W. B., Headd, J. J., Keedy, D. A., Immormino, R. M., Kapral, G. J., Murray, L. W., Richardson, J. S. & Richardson, D. C. (2010). *Acta Cryst.* D**66**, 12–21.
Dunman, P. M., Murphy, E., Haney, S., Palacios, D., Tucker-Kellogg, G., Wu, S., Brown, E. L., Zagursky, R. J., Shlaes, D. & Projan, S. J. (2001). *J. Bacteriol.* **183**, 7341–7353.
Emsley, P. & Cowtan, K. (2004). *Acta Cryst.* D**60**, 2126–2132.
Foster, T. J. (2005). *Nature Rev. Microbiol.* **3**, 948–958.
Foster, T. J. (2009). *Vet. Dermatol.* **20**, 456–470.
Foster, T. J. & Höök, M. (1998). *Trends Microbiol.* **6**, 484–488.
Hong, M., Fuangthong, M., Helmann, J. D. & Brennan, R. G. (2005). *Mol. Cell*, **20**, 131–141.
Ingavale, S. S., Van Wamel, W. & Cheung, A. L. (2003). *Mol. Microbiol.* **48**, 1451–1466.
Ishihama, A. (1993). *J. Bacteriol.* **175**, 2483–2489.
Kumarevel, T., Tanaka, T., Umehara, T. & Yokoyama, S. (2009). *Nucleic Acids Res.* **37**, 4723–4735.
Laskowski, R. A., MacArthur, M. W., Moss, D. S. & Thornton, J. M. (1993). *J. Appl. Cryst.* **26**, 283–291.
Li, D. & Cheung, A. (2008). *Infect. Immun.* **76**, 1068–1075.
Li, R., Manna, A. C., Dai, S., Cheung, A. L. & Zhang, G. (2003). *J. Bacteriol.* **185**, 4219–4225.
Liang, X., Yu, C., Sun, J., Liu, H., Landwehr, C., Holmes, D. & Ji, Y. (2006). *Infect. Immun.* **74**, 4655–4665.
Liu, X., Fujita, N., Ishihama, A. & Matsumura, P. (1995). *J. Bacteriol.* **177**, 5186–5188.
Liu, Y., Manna, A. C., Li, R., Martin, W. E., Murphy, R. C., Cheung, A. L. & Zhang, G. (2001). *Proc. Natl Acad. Sci. USA*, **98**, 6877–6882.
Liu, Y., Manna, A. C., Pan, C.-H., Kriksunov, I. A., Thiel, D. J., Cheung, A. L. & Zhang, G. (2006). *Proc. Natl Acad. Sci. USA*, **103**, 2392–2397.
Lowy, F. D. (1998). *N. Engl. J. Med.* **339**, 520–532.

Luong, T. T., Newell, S. W. & Lee, C. Y. (2003). *J. Bacteriol.* **185**, 3703–3710.
Manna, A. C. & Cheung, A. L. (2003). *Infect. Immun.* **71**, 343–353.
Manna, A. C. & Cheung, A. L. (2006). *J. Bacteriol.* **188**, 4288–4299.
Manna, A. C., Ingavale, S. S., Maloney, M., van Wamel, W. & Cheung, A. L. (2004). *J. Bacteriol.* **186**, 5267–5280.
McNamara, P. J., Milligan-Monroe, K. C., Khalili, S. & Proctor, R. A. (2000). *J. Bacteriol.* **182**, 3197–3203.
Morfeldt, E., Tegmark, K. & Arvidson, S. (1996). *Mol. Microbiol.* **21**, 1227–1237.
Murshudov, G. N., Skubák, P., Lebedev, A. A., Pannu, N. S., Steiner, R. A., Nicholls, R. A., Winn, M. D., Long, F. & Vagin, A. A. (2011). *Acta Cryst.* D**67**, 355–367.
Novick, R. P. & Geisinger, E. (2008). *Annu. Rev. Genet.* **42**, 541–564.
Poor, C. B., Chen, P. R., Duguid, E., Rice, P. A. & He, C. (2009). *J. Biol. Chem.* **284**, 23517–23524.
Ptashne, M. & Gann, A. (1997). *Nature (London)*, **386**, 569–577.
Saïd-Salim, B., Dunman, P. M., McAleese, F. M., Macapagal, D., Murphy, E., McNamara, P. J., Arvidson, S., Foster, T. J., Projan, S. J. & Kreiswirth, B. N. (2003). *J. Bacteriol.* **185**, 610–619.
Schmidt, K. A., Manna, A. C., Gill, S. & Cheung, A. L. (2001). *Infect. Immun.* **69**, 4749–4758.
Stevenson, C. E. M., Assaad, A., Chandra, G., Le, T. B. K., Greive, S. J., Bibb, M. J. & Lawson, D. M. (2013). *Nucleic Acids Res.* **41**, 7009–7022.
Sun, F., Ding, Y., Ji, Q., Liang, Z., Deng, X., Wong, C. C. L., Yi, C., Zhang, L., Xie, S., Alvarez, S., Hicks, L. M., Luo, C., Jiang, H., Lan, L. & He, C. (2012). *Proc. Natl Acad. Sci. USA*, **109**, 15461–15466.
Tseng, C. W. & Stewart, G. C. (2005). *J. Bacteriol.* **187**, 5301–5309.
Vagin, A. & Teplyakov, A. (2010). *Acta Cryst.* D**66**, 22–25.
Winn, M. D. *et al.* (2011). *Acta Cryst.* D**67**, 235–242.
Xue, T., You, Y., Shang, F. & Sun, B. (2012). *Med. Microbiol. Immunol.* **201**, 81–92.
Xue, T., Zhang, X., Sun, H. & Sun, B. (2014). *Med. Microbiol. Immunol.* **203**, 1–12.